
TCJA-SNN: Temporal-Channel Joint Attention for Spiking Neural Networks

Rui-Jie Zhu¹, Qihang Zhao², Tianjing Zhang¹,
Haoyu Deng¹, Yule Duan¹, Malu Zhang¹, Liang-Jian Deng^{1*}

¹University of Electronic Science and Technology of China

²University of Science and Technology of China

Abstract

Spiking Neural Networks (SNNs) is a practical approach toward more data-efficient deep learning by simulating neurons leverage on temporal information. In this paper, we propose the Temporal-Channel Joint Attention (TCJA) architectural unit, an efficient SNN technique that depends on attention mechanisms, by effectively enforcing the relevance of spike sequence along both spatial and temporal dimensions. Our essential technical contribution lies on: 1) compressing the spike stream into an average matrix by employing the squeeze operation, then using two local attention mechanisms with an efficient 1-D convolution to establish temporal-wise and channel-wise relations for feature extraction in a flexible fashion. 2) utilizing the Cross Convolutional Fusion (CCF) layer for modeling inter-dependencies between temporal and channel scope, which breaks the independence of the two dimensions and realizes the interaction between features. By virtue of jointly exploring and recalibrating data stream, our method outperforms the state-of-the-art (SOTA) by up to 15.7% in terms of top-1 classification accuracy on all tested mainstream static and neuromorphic datasets, including Fashion-MNIST, CIFAR10-DVS, N-Caltech 101, and DVS128 Gesture.

1 Introduction

Spiking Neural Networks (SNNs) is a valuable but challenging research area with lower energy consumption [28] and superior robustness [31] than conventional Artificial Neural Networks (ANNs), holding substantial potential in the temporal data processing. Recently, backpropagation has been introduced to SNNs [4] to improve performance, allowing various ANN modules to be included in SNNs, such as batch normalization block [38] and residual block [12]. Nonetheless, integrating an ANN-based module in an efficient and bionic manner remains a challenge.

Though considerable improvements have been seen in SNNs, it does not fully benefit from the superior representational capability of deep learning, as the unique training mode of SNNs cannot model the Spatio-temporal relationship reasonably. Zheng *et al.* [38] propose a batch normalization method among temporal dimension, solving the problems of gradient vanishing and threshold-input balance. For channel-wise, Wu *et al.* [33] propose a method called NeuNorm, which includes an auxiliary neuron to adjust the strength of the stimulus generated by the former layer. Taking advantage of channel-wise information, NeuNorm can improve performance while adding bio-plausibility by mimicking retina and nearby cells' activity. However, these methods deal with temporal and spatial information separately, limiting joint information extraction.

*Corresponding author

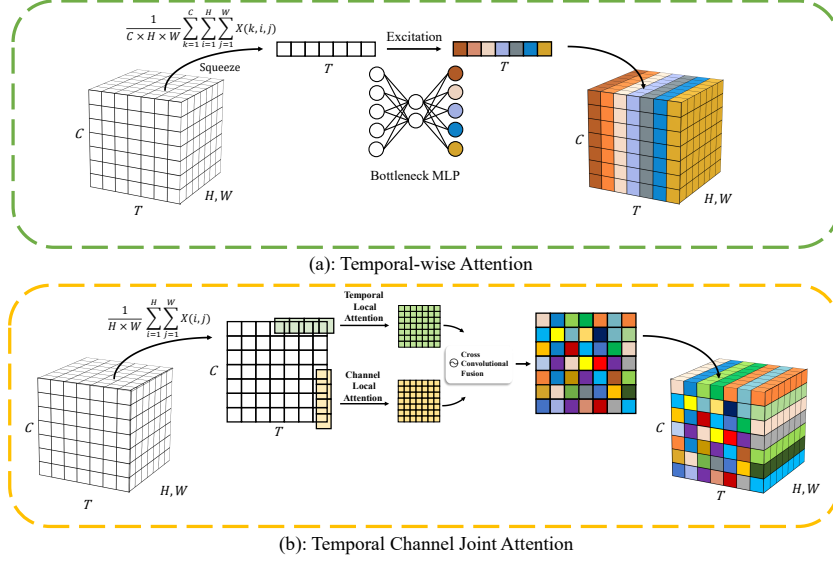


Figure 1: How our Temporal-Channel Joint Attention differs from existing temporal-wise attention [36], which estimates the saliency of each time step by squeeze-and-excitation module. T denotes the time step, C denotes the channel, and H, W represents the spatial resolution. By utilizing two separate 1-D convolutional layers and the Cross Convolutional Fusion (CCF) operation, our Temporal-Channel Joint Attention establishes the association between the time step and the channel.

The attention mechanism mimics the human ability to selectively focus on information of interest while ignoring other information, which is also worth to be explored in SNNs [36]. In [3], attention-based spike-timing-dependent plasticity SNN is proposed to address the spike-sorting problem in neuroscience. Besides, shown in Fig. 1-a, Yao *et al.* [36] attach the channel attention block to the temporal-wise input of SNN, assessing the significance over different frames during training and discarding irrelevant frames during inferencing.

In this paper, we involve both temporal and channel attention mechanisms in SNNs, which is implemented by efficient 1-D convolution; Fig. 1-b shows the whole structure, we argue that this cooperative mechanism can enhance the discrimination of the learned features.

1. We introduce a plug-and-play block into SNNs by considering the temporal and channel attentions cooperatively, which model temporal and channel information in the same phase, achieving better adaptability and bio-interpretability. To the best of our knowledge, this is the first attempt to incorporate the temporal-channel attention mechanism into the most extensively used model, LIF-based SNNs.
2. A Cross Convolutional Fusion (CCF) operation with a cross receptive field is proposed to make use of the associated information. It not only uses the benefit of convolution to minimize parameters but also integrates features from both temporal and channel dimensions in an efficient fashion.
3. TCJA-SNN is simple and easy to implement, and consistently outperforms prior methods on static Fashion-MNIST [35] datasets and neuromorphic N-Caltech 101 [25], CIFAR10-DVS [19], DVS128 Gesture [1] datasets. Specifically, we achieve 82.5% test accuracy on N-Caltech 101 dataset, substantially improving over the previously best 66.8% accuracy.

2 Related Works and Motivation

2.1 Spike-based backpropagation

In recent years, various ANN algorithms have been directly used for training deep SNNs, including gradient-descent-based algorithms. However, the non-differentiable of the spikes is the main obstacle. Specifically, the Heaviside function used to trigger the spike has a derivative that evaluates to zero

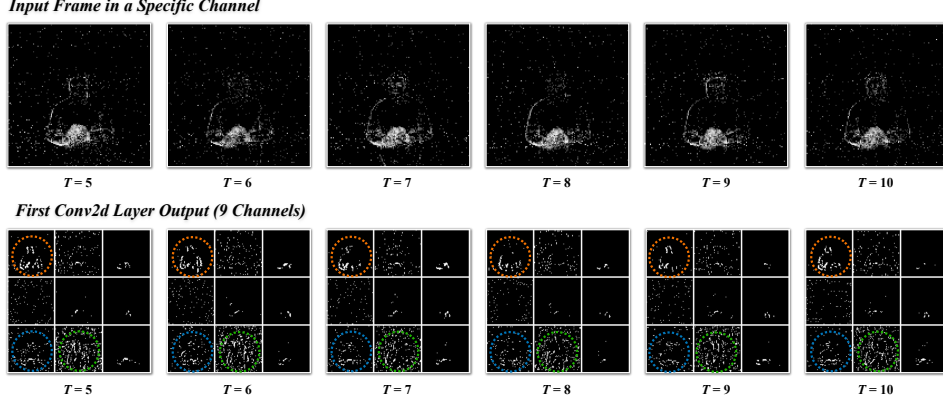


Figure 2: Correlation between proximity time steps and channels. The top row is the input frame. Each figure in the nine-pattern grid of the bottom row denotes a channel output from the first 2-D convolutional layer. It is clear that a significant correlation exists in channels with varying time steps, motivating us to merge the temporal and channel information.

everywhere but the origin, preventing gradient learning. The surrogate gradient descent method [9; 13; 23; 24; 32; 38] is a common solution to the problem. The Heaviside function is preserved during the forward pass, but a surrogate function replaces it during the backward pass. A simple choice of the surrogate function is the Spike-Operator [7], whose gradient resembles a shifted ReLU function. In this work, we take the surrogate gradient method further by introducing an ATan surrogate function and triangle-like surrogate function designed by [10] and [2], which are capable of activating a specific sample range, thus friendly to the training of deep SNNs.

2.2 Squeeze and Excitation

In ANNs, the Squeeze and Excitation (SE) block [11] has been shown as an effective module in enhancing the representation. SE can be placed into a network while only increasing a few parameters to recalibrate channel information. By squeezing and fully connecting, the trainable scale for each channel can be obtained. Recently, Yao *et al.* [36] applied the SE to formulate so-called temporal-wise attention that is effectively used in SNNs, by which the approach can figure out critical temporal frames of interest without being disturbed. Equipped with the temporal-wise attention, the given technique easily achieves the SOTA performance in various datasets, demonstrating the vast potential of the attention mechanism in SNNs.

2.3 Motivation

Based on the above analysis, the temporal-wise attention mechanism has been introduced into SNNs to learn frame-based representations for processing time-related data streams. Apart from temporal information, for spatial-wise, channel feature recalibration within convolutional layers has a high potential for performance improvement, as observed in retina cells [21] and validated in the practice of ANNs [11] and SNNs [36]. However, these works only process the data with either temporal or channel dimensions, limiting the joint feature extraction. To present the correlation between time steps and channels, we visualize the input frame and several proximity channels output from the first 2-D convolutional layer shown in Fig. 2. As circles indicated, a similar firing pattern can be distinguished from surrounding time steps and channels. To fully use this associated information, we propose the TCJA module, a novel approach for modeling temporal and channel-wise frame correlations. Furthermore, considering the inevitably increases in the model parameters caused by the attention mechanism, we attempt to adopt the 1-D convolution operation to gain a reasonable tradeoff between model performance and parameter.

3 Methodology

3.1 Leaky Integrate and Fire Model

Dating back to 1907 [18], the Leaky-Integrate-and-Fire (LIF) model accumulates the membrane voltage by integrating the external input. Compared with other biological neuron models, the LIF model consumes the lowest computational cost while possessing some biological properties, making it suitable for simulating large-scale SNNs. It can be described by a differential function [33]:

$$\tau \frac{dV(t)}{dt} = -(V(t) - V_{reset}) + I(t) \quad (1)$$

where τ denotes a time constant, $V(t)$ represents the membrane potential of the neuron at time t , and $I(t)$ represents the input from the presynaptic neurons, the product of a weight W and a spiking input $X(t)$, which accomplished by convolutional or fully-connected layer. For better computational tractability, the LIF model can be described as an explicitly iterative version [28]:

$$\begin{cases} V_t^n = H_{t-1}^n + \frac{1}{\tau}(I_{t-1}^n - (H_{t-1}^n - V_{reset})) \\ S_t^n = \Theta(V_t^n - V_{threshold}) \\ H_t^n = V_t^n \cdot (1 - S_t^n) \end{cases} \quad (2)$$

where n and t respectively represent the indices of layer and time step, τ is a time constant, V is membrane potential, S is the spiking tensor with binary value, I denotes the input from the previous layer, $\Theta(\cdot)$ denotes the Heaviside step function, H represents the reset process after spiking. As the mainstream neuron model in SNNs, the LIF model can be trained using STBP [14; 32] and surrogate gradient descent, delivering the SOTA accuracy [6; 10; 36]. The LIF model is well-suited to common machine-learning frameworks because it allows forward and backward propagation along spatial and temporal dimensions. In our method, the LIF model with $\tau = 2$, $V_{reset} = 0$ and $V_{threshold} = 1$ serves as the spiking neuron trained with the surrogate gradient descent method mentioned in Sec. 2.1.

3.2 Temporal-Channel Joint Attention (TCJA)

As mentioned above, we suggest that the frame in each time step is substantially associated with both its temporal and channel neighbors. We originally utilized the fully-connected layer to establish the correlation between temporal and channel information. However, with the increasing of channels and time steps, the number of the parameter is snowballs with a ratio of $T^2 \times C^2$ illustrated in Fig. 3. Thus, the 2-D convolutional layer is introduced to reduce the growth of parameters. The receptive field, however, is constrained by the fixed kernel size. For this reason, it is necessary to decrease the number of parameters while increasing the receptive field.

To address the mentioned difficulties, we propose a novel attention mechanism characterized by the global cross receptive field and relatively fewer parameters, named Temporal-Channel Joint Attention (TCJA), with only $T^2 + C^2$ parameters. The purpose of TCJA is to qualify the saliency score between frames and their surroundings, and the overall structure of TCJA is shown in Fig. 4. Following that, we will go over the specifics of the TCJA. First, we utilize the squeezing operation on the input frame in Sec. 3.2.1. Next, we will introduce the temporal-wise local attention (TLA) mechanism and channel-wise local attention (CLA) mechanism in Sec. 3.2.2 and Sec. 3.2.3, respectively, then propose a cross convolutional fusion (CCF) mechanism to conjointly learn the information of temporal and channel in Sec. 3.2.4.

3.2.1 Average Matrix by Squeezing

In order to efficiently capture the temporal and channel correlations between frames, we first perform the squeeze step on the spatial feature map of the input frame stream $X \in \mathbb{R}^{T \times H \times W \times C}$, where C

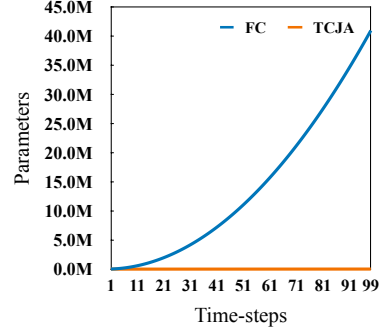


Figure 3: The growth curve of parameters between Fully-Connected (FC) layer and Temporal-Channel Joint Attention (TCJA) layer when $C = 64$.

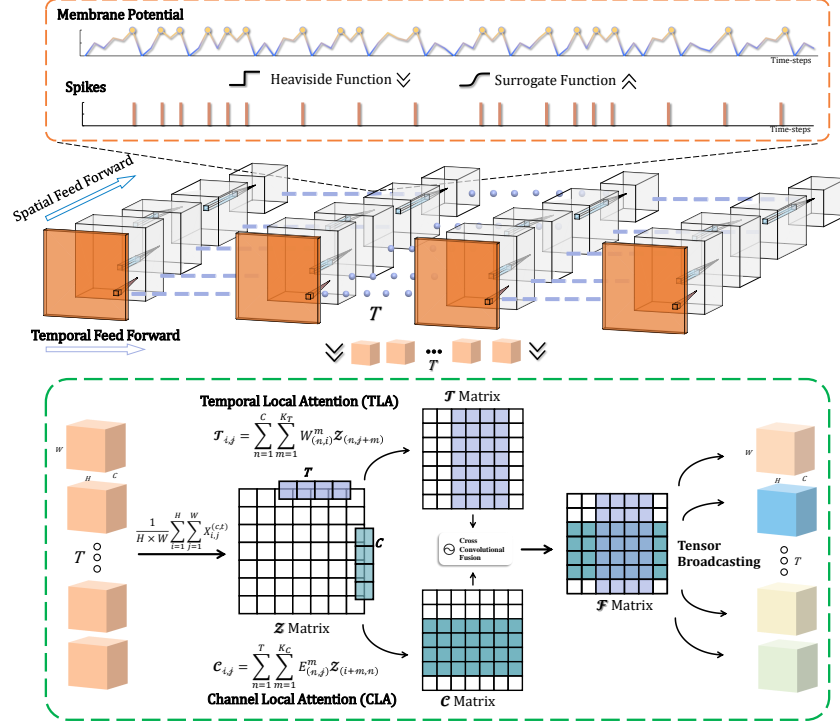


Figure 4: The Framework of SNN with TCJA module. The information flow in SNNs is a form of spike sequence along both temporal and spatial dimensions. In temporal-wise, the spiking neuron feed-forward in membrane potential (V) and spike (S) as the Eq. 2, and backpropagation with the surrogate function. In spatial-wise, data flows between layers as ANN. TCJA module first compresses the information both temporal-wise and spatial-wise, then apply TLA and CLA to establish the relationship in both temporal and channel dimensions and blend them by CCF layer.

denotes the channel size, and T denotes the time step. The squeeze step calculates an average matrix $\mathcal{Z} \in \mathbb{R}^{C \times T}$ and each element $\mathcal{Z}_{(c,t)}$ of the average matrix \mathcal{Z} is:

$$\mathcal{Z}_{(c,t)} = \frac{1}{H \times W} \sum_{i=1}^H \sum_{j=1}^W X_{i,j}^{(c,t)} \quad (3)$$

where $X^{(c,t)}$ is the input frame of c -th channel at time step t .

3.2.2 Temporal-wise Local Attention (TLA)

Following the squeeze operation, we propose the TLA mechanism for establishing temporal-wise relationships among frames. We argue that the frame in a specific time step interacts substantially with the frames in its adjacent positions. Therefore, we adopt 1-D convolution operation to model the local correspondence in the temporal dimension, as shown in Fig. 4. In detail, to capture the correlation of input frames at the temporal level, we perform C -channel 1-D convolution on each row of the average matrix \mathcal{Z} , and then accumulate the feature maps obtained by convolving different rows of the average matrix \mathcal{Z} . The whole TLA process can be described as:

$$\mathcal{T}_{i,j} = \sum_{n=1}^C \sum_{m=0}^{K_T-1} W_{(n,i)}^m \mathcal{Z}_{(n,j+m)} \quad (4)$$

where K_T ($K_T < T$) represents the size of the convolution kernel, and $W_{(n,i)}^m$ is a learnable parameter, representing the m -th parameter of the i -th channel when performing C -channel 1-D convolution on n -th row of \mathcal{Z} . $\mathcal{T} \in \mathbb{R}^{C \times T}$ is the attention score matrix after the TLA mechanism.

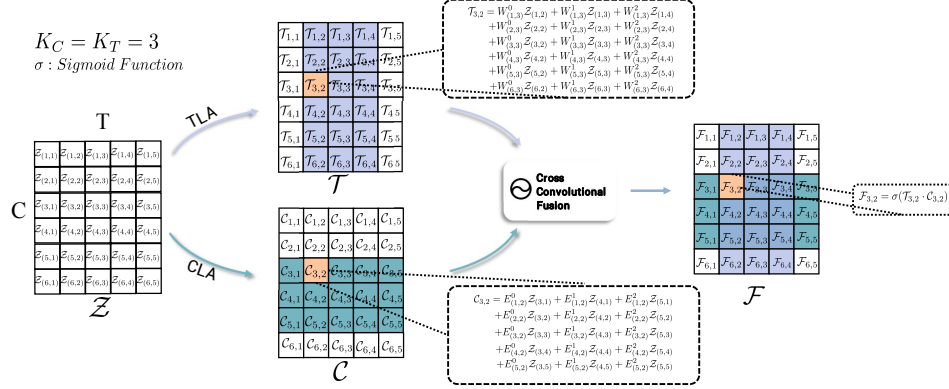


Figure 5: A Demo of TCJA. We give an average matrix $Z \in \mathbb{R}^{6 \times 5}$, and the goal of TCJA is to calculate a fusion matrix F integrating temporal and channel information. For instance, for a specific element in F : $F_{3,2}$, its calculation pipeline is as follows: 1) Calculate $T_{3,2}$ through TLA mechanism (Eq. 4); 2) Utilize CLA mechanism (Eq. 5) to calculate $C_{3,2}$, and the calculation results are shown in the black dotted box in the figure; 3) Adopt CCF mechanism (Eq. 6) to jointly learn temporal and channel information to obtain $F_{3,2}$. In addition, we can also find that after the CCF mechanism, $F_{3,2}$ integrates the information of the elements in the cross receptive field (Colored areas in F) as the anchor point, which indicates the *Cross Convolutional Fusion*.

3.2.3 Channel-wise Local Attention (CLA)

As aforementioned, the frame-to-frame saliency score should not only take into account along the temporal dimension, but also take into consideration the information from adjacent frames along the channel dimension. In order to construct the correlation of different frames with their neighbors channel-wise, we propose the CLA mechanism. Similarly, as shown in Fig. 4, we perform T -channel 1-D convolution on each column of the matrix Z , and then add the convolution results of each row, which can be described as:

$$C_{i,j} = \sum_{n=1}^T \sum_{m=0}^{K_C-1} E_{(n,j)}^m Z_{(i+m,n)} \quad (5)$$

where K_C ($K_C < C$) represents the size of the convolution kernel, and $E_{(n,i)}^m$ is a learnable parameter, representing the m -th parameter of the i -th channel when performing T -channel 1-D convolution on n -th column of Z . $C \in \mathbb{R}^{C \times T}$ is the attention score matrix after CLA mechanism.

3.2.4 Cross Convolutional Fusion (CCF)

After TLA and CLA operations, we get the temporal (TLA matrix T) and channel (CLA matrix C) saliency scores of the input frame and its adjacent frames, respectively. Next, to learn the correlation between temporal and channel frames in tandem, we propose a cross-domain information fusion mechanism, *i.e.*, the CCF layer. The goal of CCF is to calculate a fusion information matrix F , and any position (i, j) in F is used to measure the potential correlation between the i -th channel of the j -th input temporal frame and other frames.

Specifically, we can model the joint relationship between frames by element-wise multiplication of T and C . It can be described as:

$$F_{i,j} = \sigma(T_{i,j} \cdot C_{i,j}) = \sigma\left(\sum_{n=1}^C \sum_{m=0}^{K_T-1} W_{(n,i)}^m Z_{(n,j+m)} \cdot \sum_{n=1}^T \sum_{m=0}^{K_C-1} E_{(n,j)}^m Z_{(i+m,n)}\right) \quad (6)$$

where σ represents the Sigmoid function. Here, we provide a demonstration to aid comprehension of the whole computational process in Fig. 5.

3.3 Theoretical Analysis on Receptive Field

To better understand the highlights of the proposed method, we give the following theoretical analysis about the area where the network perceives and processes information during the training phase, *i.e.*, the receptive field.

Lemma 1. (Cross-Correlation Scope (CCS) of 1-D convolution) For an input feature map $I \in \mathbb{R}^{C \times T}$, if the size of the 1-D convolution kernel is defined as k , then its CCS can be described as $P \in \mathbb{R}^{k \times T}$, where the T involves the information along the second dimension of I .

Lemma 2. (CCS of two orthogonal 1-D convolution) For an input feature map $I \in \mathbb{R}^{C \times T}$, the dot multiplication of two orthogonal 1-D convolutions performed on I is equivalent to expanding the CCS into a cross shape, *i.e.*, its CCS can be described by two cross-overlaid matrices $P * Q$ (see *e.g.*, the colored area of \mathcal{F} in Fig. 5), where $P \in \mathbb{R}^{k_1 \times T}$, $Q \in \mathbb{R}^{k_2 \times C}$, and k_1 and k_2 are the size of the two convolution kernels, respectively.

Referring Eq. 6, Lemma 1, and Lemma 2, we can obtain the following corollary:

Corollary. Based on the broad CCS obtained by TCJA, there exists information flow among \mathcal{T} and \mathcal{C} , cooperatively considering the temporal and channel correlation, which is also clued in Eq. 6.

Recalling Eq. 4 and Eq. 5, through two 1-D convolutions along different dimensions, we construct two CCS in vertical relationship, which are stored in \mathcal{T} and \mathcal{C} . In particular, TCJA is to construct a CCS, which can perceive a larger area while realizing feature interaction in different directions. This cross receptive field is able to abolish the limitations caused by the monotonic dimension, thus bringing performance improvements to the network.

3.4 Training Framework

We integrate the TCJA module into the existing benchmark SNNs and propose the TCJA-SNN. Since the process of neuron firing is non-differentiable, we utilize the derived ATan surrogate function $\sigma'(x) = \frac{\alpha}{2(1+(\frac{\alpha}{2}x)^2)}$ and the derived triangle-like surrogate function $\epsilon'(x) = \frac{1}{\gamma^2} \max(0, \gamma - |x - 1|)$ for backpropagation, which is proposed by [10] and [2], respectively. We adopt spike Mean-Square-Error (SMSE) as the loss function of our TCJA-SNN as the [9; 10], which can be calculated by:

$$\mathcal{L} = \frac{1}{T} \sum_{t=0}^{T-1} \mathcal{L}_t = \frac{1}{T} \sum_{t=0}^{T-1} \frac{1}{C} \sum_{i=0}^{C-1} (s_{t,i} - g_{t,i})^2 \quad (7)$$

where T denotes the simulation time step, C is the number of labels, s represents the network output and g represents the one-hot encoded target label. To estimate the classification accuracy, we define the predicted label l_p is the index of the neuron with the highest firing rate $l_p = \max_i \frac{1}{T} \sum_{t=0}^{T-1} s_{t,i}$. Since the TCJA module simply utilizes the 1-D convolutional layer and Sigmoid function, it can be effortlessly introduced into the current network architecture as a plug-and-play module without adjusting to backpropagation.

4 Experiments

We evaluate the classification performance of TCJA-SNN on both neuromorphic datasets (CIFAR10-DVS, N-Caltech 101, and DVS128 Gesture) and static datasets (Fashion-MNIST). To verify the effectiveness of the proposed method, we integrate the TCJA module into several architectures [6; 10] with competitive performance to see if the integrated architecture can generate significant improvement. More details of the datasets, network architecture, data augmentation, and pre-process procedure can be found in the Sec. 1 and Sec. 2 of the supplementary.

4.1 Comparison with Existing SOTA Works

The performance of two TCJA-SNN variants are compared with some SOTA models in Tab. 1 and Tab. 2. We train and test two variants with SpikingJelly [8] package based on PyTorch [26] framework, resulting in enhanced performance across all tasks. Some works [9; 34; 36] substitute binary spikes with floating-point spikes in whole or in part and retain the same temporal forward pipeline as SNN to obtain improved classification accuracy. Thus, we devise two variants to validate the efficiency of

Table 1: The comparison between the proposed methods and existing SOTA techniques on three mainstream neuromorphic datasets. (Bold: the best)

| Method | Binary Spikes | CIFAR10-DVS | | N-Caltech 101 | | DVS128 | |
|--|---------------|-------------|--------------|---------------|-------------|--------|-------------|
| | | T Step | Acc. | T Step | Acc. | T Step | Acc. |
| SLAYER [29] ^{NeurIPS-2018} | ✓ | - | - | - | - | 1600 | 93.4 |
| HATS [30] ^{CVPR-2018} | N/A | N/A | 52.4 | N/A | 64.2 | - | - |
| DART [27] ^{TPAMI-2019} | N/A | N/A | 65.8 | N/A | 66.8 | - | - |
| NeuNorm [33] ^{AAAI-2019} | ✓ | 230-292 | 60.5 | - | - | - | - |
| Rollout [17] ^{Front. Neurosci-2020} | ✓ | 48 | 66.8 | - | - | 240 | 97.2 |
| DECOLLE [15] ^{Front. Neurosci-2020} | ✓ | - | - | - | - | 500 | 95.5 |
| LIAF-Net [34] ^{TNNLS-2021} | ✗ | 10 | 70.4 | - | - | 60 | 97.6 |
| tdBN [38] ^{AAAI-2021} | ✓ | 10 | 67.8 | - | - | 40 | 96.9 |
| PLIF [10] ^{ICCV-2021} | ✓ | 20 | 74.8 | - | - | 20 | 97.6 |
| TA-SNN [36] ^{ICCV-2021} | ✗ | 10 | 72.0 | - | - | 60 | 98.6 |
| SEW-ResNet [9] ^{NeurIPS-2021} | ✓ | 16 | 74.4 | - | - | 16 | 97.9 |
| Dspike [20] ^{NeurIPS-2021} | ✓ | 10 | 75.4* | - | - | - | - |
| SALT [16] ^{Neural Netw-2021} | ✓ | 20 | 67.1 | 20 | 55.0 | - | - |
| TET [6] ^{ICLR-2022} | ✗ | 10 | 83.2* | - | - | - | - |
| DSR [22] ^{CVPR-2022} | ✓ | 10 | 77.3* | - | - | - | - |
| TCJA-SNN | ✓ | 10 | 80.7* | 14 | 78.5 | 20 | 99.0 |
| TCJA-TET-SNN | ✗ | 10 | 83.3* | 14 | 82.5 | 20 | 98.2 |

* With Data Augmentation.

Table 2: Static Fashion-MNIST accuracy.

| Method | Binary Spike | Time Step | Accuracy |
|-----------------------------------|--------------|-----------|-------------|
| ST-RSBP [37] ^{NIPS-2019} | ✓ | 400 | 90.1 |
| LISNN [5] ^{IJCAI-2020} | ✓ | 20 | 92.1 |
| PLIF [10] ^{ICCV-2021} | ✓ | 8 | 94.4 |
| TCJA-SNN | ✓ | 8 | 94.8 |
| TCJA-TET-SNN | ✗ | 8 | 94.6 |

Table 3: Accuracy of different blocks.

| Block | CIFAR10-DVS | N-Caltech 101 | DVS128 |
|-------|-------------|---------------|--------|
| TLA | 79.7 | 78.3 | 97.9 |
| CLA | 80.5 | 78.4 | 98.6 |
| TCJA | 80.7 | 78.5 | 99.0 |

TCJA-SNN by utilizing the Temporal Efficient Training (TET) [6]. On CIFAR10-DVS, we obtain 3.4% advantage over the prior method with binary spikes. On N-Caltech 101, with only 14 time steps, we get a 15.7% increase over the prior best work. On DVS128, we get an accuracy of 99.0%, which is higher than TA-SNN [36] using three times fewer simulation time steps. Furthermore, by using a basic 7-layer CNN on the static dataset Fashion MNIST, our method can achieve the highest classification accuracy with the fewest simulation time steps. Overall, with binary spikes, TCJA-SNN simulates no-more time steps while getting a higher performance. Furthermore, our method can achieve higher classification accuracy by adopting the non-binary spike technique.

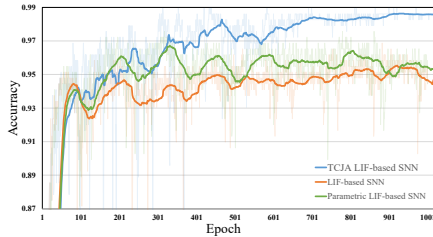


Figure 6: Convergence of compared SNN methods on DVS128 Gesture.

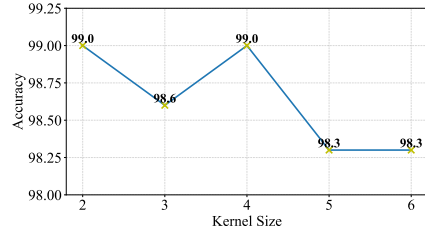


Figure 7: Variation in test accuracy on DVS128 Gesture dataset as kernel size increases.

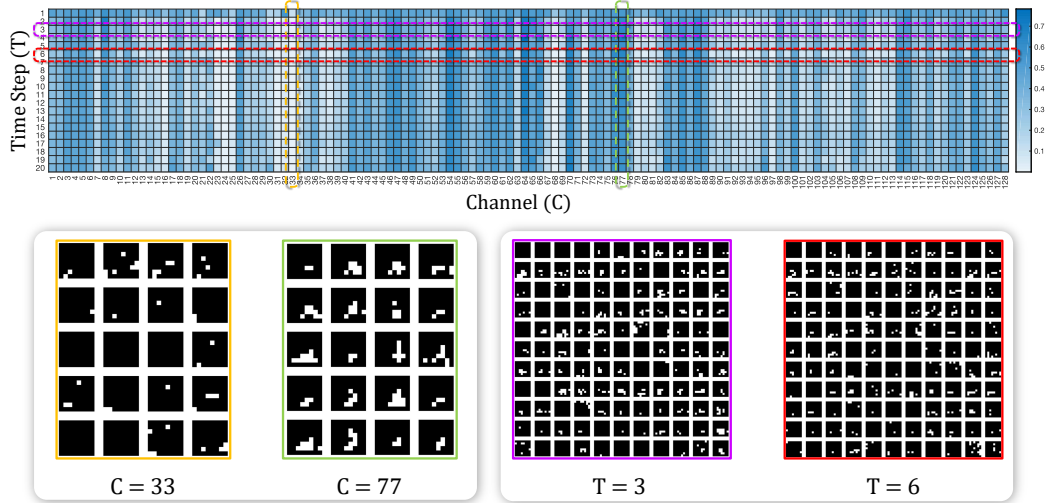


Figure 8: Attention distribution between time step and channel. The top row is the weight from the first TCJA module in TCJA-SNN working with DVS128 Gesture dataset. We select sparse and dense attention frames in both temporal-wise ($T = 1, 6$) and channel-wise ($C = 33, 77$) in bottom row.

4.2 Ablation Study and Discussions

Ablation Study. To investigate the influence of the TLA and the CLA modules, we conduct several ablation studies. As shown in Tab. 3, the CLA module contributes significantly to performance enhancement. This is because simulation time steps are much fewer than channels in most SNNs designs, allowing the CLA module to extract extra relevant features than TLA. Notably, the TCJA module exhibits improved performance across all datasets examined, demonstrating the effectiveness of the CCF layer.

Discussion of Kernel Size. We initially investigate the kernel size in TCJA module. Intuitively, when the size of the kernel rises, the receptive field of the local attention mechanism will also expand, which may aid in enhancing the performance of TCJA-SNN. However, the experimental results in Fig. 7 overturn this conjecture. As the size of the kernel rises, the performance of the model waves. When the kernel size is less than 4, the model achieves the optimal effect. One reasonable explanation is that a frame mainly correlates with its nearby frames, and an excessively large receptive field may lead to undesired noise.

Discussion of Convergence. We also empirically demonstrate the convergence of our proposed method, as shown in Fig. 6. Specifically, the Fig. 6 illustrates the performance trend of vanilla LIF-SNN, PLIF [10] and our proposed TCJA-SNN for 1000 epochs. As the training epoch increases, the performance trend of our proposed method becomes more stable and converges to a higher level. Moreover, the TCJA-SNN can achieve the SOTA performance when only training about 260 epochs, which demonstrates the efficacy of the proposed TCJA.

Discussions of Attention Visualization. To make the attention mechanism easier to understand, we finally visualize the output of the first TCJA module in TCJA-SNN working with DVS128 Gesture dataset, which can be seen in Fig. 8. Changes in attention weights are primarily accumulated among channels, verifying further the substantial role performed by the CLA in the TCJA module. To embody the attention weights, we extract some temporal-wise and channel-wise frames. The difference in firing pattern in the channel dimension is more significant than that in the temporal dimension. Further discussions can be found in Sec. 3 of the supplementary.

5 Conclusion

In this paper, we propose the TCJA mechanism, which innovatively recalibrates temporal and channel information in SNN. Specifically, instead of utilizing a generic fully connected network, we use 1-D convolution to build the correlation between frames, reducing the computation and improving model

performance. Moreover, we propose a CCF mechanism to realize joint feature interaction between temporal and channel information. Sufficient experiments verify the effectiveness of our method with SOTA results on four datasets, *i.e.*, CIFAR10-DVS (83.3%), N-Caltech101 (82.5%), DVS128 (99.0%) and Fashion-MNIST (94.8%). However, the insertion of TCJA still resulted in a relatively sizable boost in the number of parameters, which can be found in Sec. 3 of the supplementary. In the future work, we believe this method can easily be integrated into the neuromorphic chip for the hardware-friendly 1-D convolution operation and the binary spiking network structure.

References

- [1] Arnon Amir, Brian Taba, David Berg, and et al. A Low Power, Fully Event-Based Gesture Recognition System. In *Proceedings of the IEEE/CVF Conference on Computer Vision and Pattern Recognition (CVPR)*, 2017.
- [2] Guillaume Bellec, Darjan Salaj, Anand Subramoney, Robert Legenstein, and Wolfgang Maass. Long short-term memory and learning-to-learn in networks of spiking neurons. In *Advances in Neural Information Processing Systems (NeurIPS)*, volume 31, 2018.
- [3] Marie Bernert and Blaise Yvert. An Attention-Based Spiking Neural Network for Unsupervised Spike-Sorting. *International Journal of Neural Systems*, 29(8):1850059:1–1850059:19, 2019.
- [4] Sander M. Bohtë, Joost N. Kok, and Johannes A. La Poutre. Error-backpropagation in Temporally Encoded Networks of Spiking Neurons. *Neurocomputing*, 48(1-4):17–37, 2002.
- [5] Xiang Cheng, Yunzhe Hao, Jiaming Xu, and Bo Xu. LISNN: Improving Spiking Neural Networks with Lateral Interactions for Robust Object Recognition. In *International Joint Conference on Artificial Intelligence (IJCAI)*, pages 1519–1525, 2020.
- [6] Shikuang Deng, Yuhang Li, Shanghang Zhang, and Shi Gu. Temporal Efficient Training of Spiking Neural Network via Gradient Re-weighting. In *International Conference on Learning Representations (ICLR)*, 2021.
- [7] Jason K. Eshraghian, Max Ward, Emre Neftci, Xinxin Wang, Gregor Lenz, Girish Dwivedi, Mohammed Bennis, Doo Seok Jeong, and Wei D. Lu. Training Spiking Neural Networks Using Lessons From Deep Learning. *ArXiv*, 2021.
- [8] Wei Fang, Yanqi Chen, Jianhao Ding, Ding Chen, Zhaofei Yu, Huihui Zhou, Yonghong Tian, and other contributors. Spikingjelly. <https://github.com/fangwei123456/spikingjelly>, 2020. Accessed: 2022-05-04.
- [9] Wei Fang, Zhaofei Yu, Yanqi Chen, Tiejun Huang, Timothée Masquelier, and Yonghong Tian. Deep Residual Learning in Spiking Neural Networks. In *Advances in Neural Information Processing Systems (NeurIPS)*, volume 34, pages 21056–21069, 2021.
- [10] Wei Fang, Zhaofei Yu, Yanqi Chen, Timothée Masquelier, Tiejun Huang, and Yonghong Tian. Incorporating Learnable Membrane Time Constant To Enhance Learning of Spiking Neural Networks. In *Proceedings of the IEEE/CVF International Conference on Computer Vision (ICCV)*, pages 2661–2671, 2021.
- [11] Jie Hu, Li Shen, and Gang Sun. Squeeze-and-Excitation Networks. In *Proceedings of the IEEE Conference on Computer Vision and Pattern Recognition (CVPR)*, 2018.
- [12] Yangfan Hu, Huajin Tang, and Gang Pan. Spiking Deep Residual Networks. *IEEE Transactions on Neural Networks and Learning Systems*, pages 1–6, 2018.
- [13] Cheng Jin, Rui-Jie Zhu, Xiao Wu, and Liang-Jian Deng. SIT: A Bionic and Non-Linear Neuron for Spiking Neural Network. *ArXiv preprint arXiv:2203.16117*, 2022.
- [14] Yingyezhe Jin, Wenrui Zhang, and Peng Li. Hybrid Macro/Micro Level Backpropagation for Training Deep Spiking Neural Networks. In *Advances in Neural Information Processing Systems (NeurIPS)*, volume 31, 2018.
- [15] Jacques Kaiser, Hesham Mostafa, and Emre Neftci. Synaptic Plasticity Dynamics for Deep Continuous Local Learning (DECOLLE). *Frontiers in Neuroscience*, 14:424, 2020.

- [16] Youngeun Kim and Priyadarshini Panda. Optimizing Deeper Spiking Neural Networks for Dynamic Vision Sensing. *Neural Networks*, 144:686–698, 2021.
- [17] Alexander Kugele, Thomas Pfeil, Michael Pfeiffer, and Elisabetta Chicca. Efficient Processing of Spatio-temporal Data Streams with Spiking Neural Networks. *Frontiers in Neuroscience*, 14:439, 2020.
- [18] Louis Lapique. Recherches quantitatives sur l’excitation électrique des nerfs traitée comme une polarisation. *Journal of Physiology and Pathology*, 9:620–635, 1907.
- [19] Hongmin Li, Hanchao Liu, Xiangyang Ji, Guoqi Li, and Luping Shi. CIFAR10-DVS: An Event-Stream Dataset for Object Classification. *Frontiers in Neuroscience*, 11:309, 2017.
- [20] Yuhang Li, Yufei Guo, Shanghang Zhang, Shikuang Deng, Yongqing Hai, and Shi Gu. Differentiable Spike: Rethinking Gradient-Descent for Training Spiking Neural Networks. In *Advances in Neural Information Processing Systems (NeurIPS)*, volume 34, pages 23426–23439, 2021.
- [21] Valerio Mante, Vincent Bonin, and Matteo Carandini. Functional mechanisms shaping lateral geniculate responses to artificial and natural stimuli. *Neuron*, 58(4):625–638, 2008.
- [22] Qingyan Meng, Mingqing Xiao, Shen Yan, Yisen Wang, Zhouchen Lin, and Zhi-Quan Luo. Training High-Performance Low-Latency Spiking Neural Networks by Differentiation on Spike Representation. *ArXiv preprint arXiv:2205.00459*, 2022.
- [23] Emre O. Neftci, Hesham Mostafa, and Friedemann Zenke. Surrogate Gradient Learning in Spiking Neural Networks: Bringing the Power of Gradient-Based Optimization to Spiking Neural Networks. *IEEE Signal Processing Magazine*, 36(6):51–63, 2019.
- [24] Emre O Neftci, Hesham Mostafa, and Friedemann Zenke. Surrogate Gradient Learning in Spiking Neural Networks: Bringing the Power of Gradient-Based Optimization to Spiking Neural Networks. *IEEE Signal Processing Magazine*, 36(6):51–63, 2019.
- [25] Garrick Orchard, Ajinkya Jayawant, Gregory K Cohen, and Nitish Thakor. Converting Static Image Datasets to Spiking Neuromorphic Datasets Using Saccades. *Frontiers in Neuroscience*, 9:437, 2015.
- [26] Adam Paszke, Sam Gross, Francisco Massa, Adam Lerer, James Bradbury, Gregory Chanan, Trevor Killeen, Zeming Lin, Natalia Gimelshein, Luca Antiga, Alban Desmaison, Andreas Kopf, Edward Yang, Zachary DeVito, Martin Raison, Alykhan Tejani, Sasank Chilamkurthy, Benoit Steiner, Lu Fang, Junjie Bai, and Soumith Chintala. PyTorch: An Imperative Style, High-Performance Deep Learning Library. In *Advances in Neural Information Processing Systems (NeurIPS)*, volume 32, 2019.
- [27] Bharath Ramesh, Hong Yang, Garrick Orchard, Ngoc Anh Le Thi, Shihao Zhang, and Cheng Xiang. DART: Distribution Aware Retinal Transform for Event-Based Cameras. *IEEE Transactions on Pattern Analysis and Machine Intelligence*, 42(11):2767–2780, 2019.
- [28] Kaushik Roy, Akhilesh Jaiswal, and Priyadarshini Panda. Towards spike-based machine intelligence with neuromorphic computing. *Nature*, 575(7784):607–617, 2019.
- [29] Sumit Bam Shrestha and Garrick Orchard. SLAYER: Spike Layer Error Reassignment in Time. In *Advances in Neural Information Processing Systems (NeurIPS)*, volume 31, 2018.
- [30] Amos Sironi, Manuele Brambilla, Nicolas Bourdis, Xavier Lagorce, and Ryad Benosman. HATS: Histograms of Averaged Time Surfaces for Robust Event-Based Object Classification. In *Proceedings of the IEEE/CVF Conference on Computer Vision and Pattern Recognition (CVPR)*, pages 1731–1740, 2018.
- [31] Evangelos Stamatias, Daniel Neil, Michael Pfeiffer, Francesco Galluppi, Steve B Furber, and Shih-Chii Liu. Robustness of spiking Deep Belief Networks to noise and reduced bit precision of neuro-inspired hardware platforms. *Frontiers in Neuroscience*, 9:222, 2015.
- [32] Yujie Wu, Lei Deng, Guoqi Li, Jun Zhu, and Luping Shi. Spatio-Temporal Backpropagation for Training High-performance Spiking Neural Networks. *Frontiers in neuroscience*, 12:331, 2018.

- [33] Yujie Wu, Lei Deng, Guoqi Li, Jun Zhu, Yuan Xie, and Luping Shi. Direct Training for Spiking Neural Networks: Faster, Larger, Better. In *Proceedings of the AAAI Conference on Artificial Intelligence (AAAI)*, pages 1311–1318, 2019.
- [34] Zhenzhi Wu, Hehui Zhang, Yihan Lin, Guoqi Li, Meng Wang, and Ye Tang. LIAF-Net: Leaky Integrate and Analog Fire Network for Lightweight and Efficient Spatiotemporal Information Processing. *IEEE Transactions on Neural Networks and Learning Systems*, pages 1–14, 2021.
- [35] Han Xiao, Kashif Rasul, and Roland Vollgraf. Fashion-mnist: a Novel Image Dataset for Benchmarking Machine Learning Algorithms. *ArXiv preprint arXiv:1708.07747*, 2017.
- [36] Man Yao, Huanhuan Gao, Guangshe Zhao, Dingheng Wang, Yihan Lin, Zhao-Xu Yang, and Guoqi Li. Temporal-wise Attention Spiking Neural Networks for Event Streams Classification. In *Proceedings of the IEEE/CVF International Conference on Computer Vision (ICCV)*, pages 10201–10210, 2021.
- [37] Wenrui Zhang and Peng Li. Spike-Train Level Backpropagation for Training Deep Recurrent Spiking Neural Networks. In *Advances in Neural Information Processing Systems (NeurIPS)*, volume 32, 2019.
- [38] Hanle Zheng, Yujie Wu, Lei Deng, Yifan Hu, and Guoqi Li. Going Deeper With Directly-Trained Larger Spiking Neural Networks. In *Proceedings of the AAAI Conference on Artificial Intelligence (AAAI)*, pages 11062–11070, 2021.

Checklist

1. For all authors...
 - (a) Do the main claims made in the abstract and introduction accurately reflect the paper’s contributions and scope? **[Yes]** Our abstract and introduction clearly describe our contribution, the algorithm, and the experimental results.
 - (b) Did you describe the limitations of your work? **[Yes]** We mentioned our limitation in Sec. 5 and analyze it in Sec. 3 of the supplementary.
 - (c) Did you discuss any potential negative societal impacts of your work? **[No]** This work is a theoretical research in spiking neural networks. For the time being, it does not present any foreseeable negative societal impact.
 - (d) Have you read the ethics review guidelines and ensured that your paper conforms to them? **[Yes]**
2. If you are including theoretical results...
 - (a) Did you state the full set of assumptions of all theoretical results? **[Yes]** All assumptions are stated in Sec. 3.3.
 - (b) Did you include complete proofs of all theoretical results? **[Yes]** All proofs are provided in Sec. 3.3.
3. If you ran experiments...
 - (a) Did you include the code, data, and instructions needed to reproduce the main experimental results (either in the supplemental material or as a URL)? **[Yes]** Our code will be available in the supplementary material.
 - (b) Did you specify all the training details (e.g., data splits, hyperparameters, how they were chosen)? **[Yes]** See Sec. 2 of the supplementary.
 - (c) Did you report error bars (e.g., with respect to the random seed after running experiments multiple times)? **[No]** Testing our model is time-consuming on our servers and we lack sufficient resources/time for multiple repetitions for our experiments.
 - (d) Did you include the total amount of compute and the type of resources used (e.g., type of GPUs, internal cluster, or cloud provider)? **[Yes]** The computational resources are shown in Sec .2 of the supplementary.
4. If you are using existing assets (e.g., code, data, models) or curating/releasing new assets...
 - (a) If your work uses existing assets, did you cite the creators? **[Yes]** We use DVS128 Gesture [1], CIFAR10-DVS [19], N-Caltech 101 [25], and Fashion-MNIST [35] datasets.

- (b) Did you mention the license of the assets? [No] We adopt public datasets.
 - (c) Did you include any new assets either in the supplemental material or as a URL? [No]
 - (d) Did you discuss whether and how consent was obtained from people whose data you're using/curating? [No]
 - (e) Did you discuss whether the data you are using/curating contains personally identifiable information or offensive content? [No]
5. If you used crowdsourcing or conducted research with human subjects...
- (a) Did you include the full text of instructions given to participants and screenshots, if applicable? [N/A]
 - (b) Did you describe any potential participant risks, with links to Institutional Review Board (IRB) approvals, if applicable? [N/A]
 - (c) Did you include the estimated hourly wage paid to participants and the total amount spent on participant compensation? [N/A]

TCJA-SNN: Temporal-Channel Joint Attention for Spiking Neural Networks

Anonymous Author(s)

Affiliation

Address

email

1 In this supplementary, We begin with a further description of the datasets, including dataset pre-
 2 processing and data augmentation. After then, more details on the training’s implementation are
 3 provided. Finally, the time and space complexity, the fusion operation, and network parameters are
 4 discussed.

5 1 Detail of Datasets

6 1.1 Dataset Introduction

7 We have conducted experiments on both event-stream and static datasets for object classification. The
 8 summaries of datasets involved in the experiment are listed below.

- 9 • **CIFAR10-DVS** The CIFAR10-DVS [?] dataset is an adapted event-driven version from
 10 the popular static dataset CIFAR10. This dataset converts 10,000 frame-based images of 10
 11 classes into event streams with the dynamic vision sensor. Since the CIFAR10-DVS dataset
 12 does not divide training and testing sets, we split the dataset into 9k training images and 1k
 13 test images and reduced the spatial resolution from 128×128 to 48×48 as [? ? ? ?].
- 14 • **N-Caltech 101** The N-Caltech 101 [?] dataset is also converted from the original version
 15 of Caltech 101 [?] with a slight change in object classes to avoid confusion. The N-Caltech
 16 101 consists of 100 object classes plus one background class. We apply the 9: 1 train-test
 17 split as CIFAR10-DVS.
- 18 • **DVS128 Gesture** The DVS128 Gesture [?] dataset is an event-stream dataset composed
 19 of 11 kinds of hand gestures from 29 subjects under three different illumination conditions,
 20 directly captured with the DVS128 camera.
- 21 • **Fashion-MNIST** The Fashion-MNIST [?] is a tiny but demanding static dataset designed
 22 to serve as a straight replacement for the original MNIST dataset for more complicated
 23 visual patterns. The Fashion-MNIST dataset contains 70,000 grayscale images of 10 kinds
 24 of fashion products, all in a 28×28 size.

25 1.2 Neuromorphic Datasets Preprocessing

26 We use the integrating approach to convert event stream to frame data, which is commonly used in
 27 SNNs[? ? ? ?], to preprocess neuromorphic datasets. The coordinate of event can be describe as:

$$E(x_i, y_i, p_i) \quad (1)$$

28 where x_i and y_i event’s coordinate, p_i represents the event. In order to reduce computational
 29 consumption, we group events into T slices, where T is the network’s time simulation step. The

process can be describe as:

$$\begin{aligned}
j_l &= \left\lfloor \frac{N}{T} \right\rfloor \cdot j \\
j_r &= \begin{cases} \left\lfloor \frac{N}{T} \right\rfloor \cdot (j+1) & \text{if } j < T-1 \\ N & \text{if } j = T-1 \end{cases} \\
F(j, p, x, y) &= \sum_{i=j_l}^{j_r-1} \mathcal{I}_{p,x,y}(p_i, x_i, y_i)
\end{aligned} \tag{2}$$

where $\lfloor \cdot \rfloor$ is the floor operation, and $\mathcal{I}_{p,x,y}(p_i, x_i, y_i)$ is an indicator function and it equals 1 only when $(p, x, y) = (p_i, x_i, y_i)$.

1.3 Data Augmentation

To mitigate the apparent overfitting on the CIFAR10-DVS dataset, we adopt the neuromorphic data augmentation, which is also used in [?] for training the same dataset. We follow the same augmentation setting as [?]: we utilize horizontal Flipping and Mixup [?] in each frame, where probability of Flipping is set to 0.5, and the Mixup interpolation factor is sampled from $\beta(0.5, 0.5)$. Then, we randomly select one augmentation among Rolling, Rotation, Cutout, and Shear, where random Rolling range is 5 pixels, the degree of Rotation is sampled from the uniform distribution $\mathcal{U}(-15, 15)$, the side length of Cutout is sampled from the uniform distribution $\mathcal{U}(1, 8)$, and the shear degree is also sampled from the uniform distribution $\mathcal{U}(-8, 8)$.

2 Training Details

2.1 Network Architecture

The network architectures designed for the different datasets are listed in Tab. 1.

Table 1: The network architecture setting for each dataset. $x\text{Cy}/\text{MPy}/\text{APy}$ denotes is the Conv2D/MaxPooling/AvgPooling layer with output channels = x and kernel size = y . All convolutional layer step sizes are set to 1 (including Conv1D layer in TCJA, TLA, and CLA). $n\text{FC}$ denotes the fully connected layer with output feature = n , $m\text{DP}$ is the spiking dropout layer with dropout ratio m .

| Dataset | Network Architecture |
|----------------|---|
| DVS128 Gesture | 128C3-LIF-MP2-128C3-LIF-MP2-128C3-LIF-MP2-128C3-LIF-MP2-0.5DP-512FC-LIF-0.5DP-100FC-LIF-Voting |
| CIFAR10-DVS | 64C3-LIF-128C3-LIF-AP2-256C3-LIF-256C3-LIF-AP2-512C3-LIF-512C3-LIF-AP2-512C3-LIF-512C3-LIF-AP2-10FC-LIF |
| N-Caltech 101 | 64C3-LIF-MP2-128C3-LIF-MP2-256C3-LIF-MP2-256C3-LIF-MP2-512C3-LIF-0.8DP-1024FC-LIF-0.5DP-101FC-LIF |
| Fashion-MNIST | 128C3-LIF-AP2-128C3-LIF-AP2-0.5DP-512FC-LIF-0.5DP-10FC-LIF |

For DVS128 dataset, we utilize the same network structure and hyper-parameters as the [?] and add the TCJA module before last two pooling layers. Dropout (DP) [?] rate is set to 0.5 in accordance with the original network. We add a 1-D average pooling voting layer in the last layer, which yielded a 10-dimensional vector as the vote outcome. This is because the preprocess of DVS128 Gesture simulates a longer timestep ($T=20$), through such a voting layer the robustness of the network can be improved [?].

For CIFAR10-DVS dataset, we adopt VGG11-like architecture introduced in TET [?]. Due to the significant overfitting, we adopt the data augmentation as [?] and [?]. To maintain the same training settings as [?] for TCJA-TET-SNN, we use the triangle surrogate function, eliminate the last LIF layer, and replace the SMSE loss with TET loss. For TCJA-SNN, the TCJA module is added before

the last two pooling layers, and for TCJA-TET-SNN, the TCJA module is included before the first pooling layer as the replacement of surrogate function and loss.

For N-Caltech 101 dataset, we combine two architectures together and add the TCJA module before last two pooling layers. We first reserve a pooling for each layer; then, with the network going deeper, spatial resolution is reduced with the increasing channel number. To relieve the evident overfitting, the ratio of the first dropout layer is increased to 0.8.

For Fashion-MNIST dataset, we follow the network structure from [?]. Note that the first convolutional layer is a static encoding layer, transforming the static image into spikes.

2.2 Network Implementation

We train and test our method on a workstation equipped with two Tesla P4 and two Tesla P10 GPUs. As the memory consumption, we use the Tesla P10 to training and testing CIFAR10-DVS dataset, N-Caltech 101 dataset, and DVS128 Gesture dataset, and use the Tesla P4 to training and testing Fashion-MNIST dataset. For different datasets, hyperparameters are listed in Tab. 2.

Table 2: Hyperparameter settings of TCJA-SNN.

| Hyperparameter | CIFAR10-DVS | N-Caltech 101 | DVS128 | Fashion-MNIST |
|---------------------------|-------------|---------------|--------------|---------------|
| Learning Rate | $1e-3$ | $1e-3$ | $1e-3$ | $1e-3$ |
| Batch Size | 64 | 32 | 16 | 128 |
| T | 10 | 14 | 20 | 8 |
| Automatic Mixed Precision | \times | \checkmark | \checkmark | \times |
| Training Epochs | 1000 | 500 | 1000 | 1000 |

We set the learning rate to $1e-3$ in each dataset empirically, and train the same epochs as [?] except N-Caltech 101, which is not tested in [?]. we enable the automatic mixed precision in N-Caltech 101 and DVS128 Gesture for the excessive resolution (180×240 and 128×128). We also detach the reset process in backpropagation, which is validated to enhance performance.

3 Further Discussions

3.1 Complexity Analysis

Finally, we try to analyze the time and space complexity of TLA and CLA. For TLA, Recall the Eq. 3 in the main manuscript for calculating each element:

$$\mathcal{T}_{i,j} = \sum_{n=1}^C \sum_{m=0}^{K_T-1} W_{(n,i)}^m \mathcal{Z}_{(n,j+m)} \quad (3)$$

where K_T ($K_T < T$) represents the size of the convolution kernel, and $W_{(n,i)}^m$ is a learnable parameter, representing the m -th parameter of the i -th channel when performing C -channel 1-D convolution on n -th row of \mathcal{Z} . $\mathcal{T} \in \mathbb{R}^{C \times T}$ is the attention score matrix after the TLA mechanism.

The time complexity of obtaining each element of \mathcal{T} is $\mathcal{O}(CK)$ (K : Kernel size). Consequently, the time complexity of the whole TLA mechanism is $\mathcal{O}(TC^2K)$. Moreover, the space complexity is composed of the parameters and the memory occupied by variables. On the one hand, for the parameters, C -channel 1-D convolution is performed on each row of \mathcal{Z} , so the total amount of parameters required is $C * C * K$, on the other hand, for variables, in the whole process, we only need to maintain a matrix of dimension $C \times T$. In conclusion, the space complexity is $\mathcal{O}(C^2K + CT)$. Similarly, for CLA, the time complexity is $\mathcal{O}(T^2CK)$ and the space complexity is $\mathcal{O}(T^2K + CT)$.

Table 3: Test accuracy on three datasets with different CCF operation.

| Type | CIFAR10-DVS | N-Caltech 101 | DVS128 |
|----------------|-------------|---------------|--------|
| Addition | 80.7 | 78.0 | 98.2 |
| Multiplication | 80.7 | 78.5 | 99.0 |

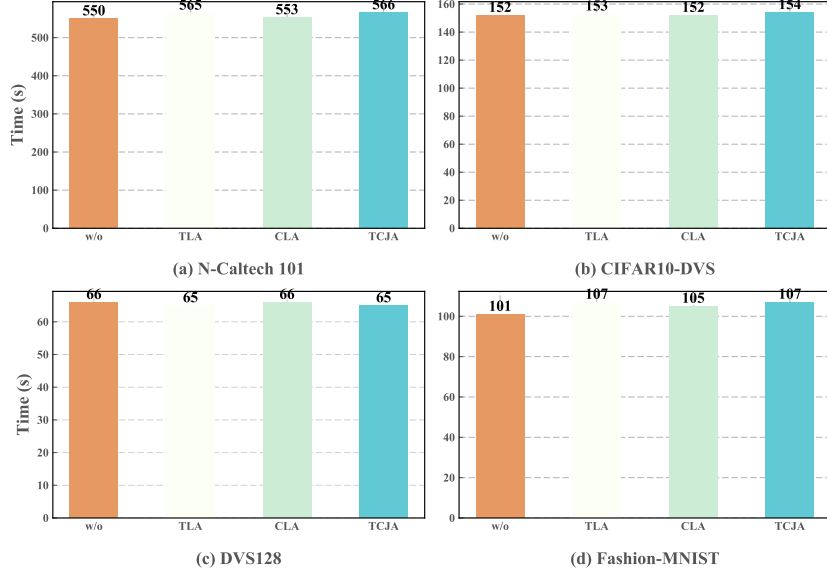


Figure 1: A comparison of the running time executing the various modules. All of the experiments are conducted in Tesla P10 and Tesla P4 as the Sec. 2.2.

3.2 Multiplication vs. Addition

To verify the effectiveness of our proposed CCF mechanism, we devise a variant method that substitutes addition for multiplication of $\mathcal{T}_{i,j}$ and $\mathcal{C}_{i,j}$ in CCF layer, which can be described as:

$$\mathcal{F}_{i,j} = \sigma(\mathcal{T}_{i,j} \cdot \mathcal{C}_{i,j}) = \sigma\left(\sum_{n=1}^C \sum_{m=0}^{K_T-1} W_{(n,i)}^m \mathcal{Z}_{(n,j+m)} + \sum_{n=1}^T \sum_{m=0}^{K_C-1} E_{(n,j)}^m \mathcal{Z}_{(i+m,n)}\right) \quad (4)$$

where σ represents the Sigmoid function. The results are shown in the Tab. 3. As we observed, the addition operation achieves a good performance, However, as compared to the multiplication operation, the final computation result is worse since it lacks the cross term, which inhibits a firm formulation of the correlation between frames.

3.3 Trainable Parameter Analysis

Table 4: The increase of TLA, CLA and TCJA module on the amount of model parameters. An intuitive impression is that CLA has little effect on the amount of model parameters, while the insertion of TLA and TCJA lead to a significant increase in the amount of model parameters.

| Datasets | TLA | CLA | TCJA |
|----------------|---------|--------|---------|
| CIFAR10-DVS | 22.648% | 0.009% | 22.669% |
| N-Caltech 101 | 9.472% | 0.007% | 9.479% |
| DVS128 Gesture | 7.754% | 0.189% | 7.943% |
| Fashion-MNIST | 1.948% | 0.008% | 1.955% |

94 We also give the effects of TLA, CLA, and TCJA on the increase of model parameters, as shown in
95 the Tab. 3.3. First, with different datasets, the proportion of different modules to the number of model
96 parameters varies. The increase of TLA and TCJA to the number of parameters is much higher than
97 that of CLA. This phenomenon is consistent with our expectations that given that the channel size in
98 the dataset is much larger than the simulation time step, indicating that CLA has a small number of
99 parameters. Secondly, combined with the analyses of the Sec. ?? (*Ablation Study*) and the discussion
100 of the Sec. ?? (*Discussions of Attention Visualization*) in the main manuscript, we may conclude
101 that CLA has a significant role in enhancing the model’s performance. In practical application, we
102 can thus make a trade-off based on the actual situation: while considering energy consumption, we
103 can only use the CLA mechanism in the model, but when an accuracy guarantee is required, the
104 TCJA mechanism can be utilized. However, due to the efficient implementation of convolution, our
105 approach does not need additional training time, which can be seen in Fig. 1.